Pan-cancer transcriptional signatures predictive of oncogenic mutations reveal that Fbw7 regulates cancer cell oxidative metabolism

Ryan J. Davis[a,b,c,1], Mehmet Gönen[d,e,f,1], Daciana H. Margineantu[a,b,1], Shlomo Handeli[a,b], Jherek Swanger[a,b], Pia Hoellerbauer[a], Patrick J. Paddison[a], Haiwei Gu[g,h], Daniel Raftery[g,h], Jonathan E. Grim[b], David M. Hockenbery[a,b,2], Adam A. Margolin[d,2], and Bruce E. Clurman[a,b,2,3]

[a]Division of Human Biology, Fred Hutchinson Cancer Research Center, Seattle, WA 98109; [b]Division of Clinical Research, Fred Hutchinson Cancer Research Center, Seattle, WA 98109; [c]Molecular and Cellular Biology Graduate Program, University of Washington, Seattle, WA 98195; [d]Department of Biomedical Engineering, Oregon Health & Science University, Portland, OR 97239; [e]Department of Industrial Engineering, College of Engineering, Koç University, 34450 Istanbul, Turkey; [f]School of Medicine, Koç University, 34450 Istanbul, Turkey; [g]Northwest Metabolomics Research Center, University of Washington, Seattle, WA 98109; and [h]Division of Public Health Sciences, Fred Hutchinson Cancer Research Center, Seattle, WA 98109

Edited by William G. Kaelin, Jr., Dana-Farber Cancer Institute and Brigham and Women's Hospital, Harvard Medical School, Boston, MA, and approved April 6, 2018 (received for review October 19, 2017)

The Fbw7 (F-box/WD repeat-containing protein 7) ubiquitin ligase targets multiple oncoproteins for degradation and is commonly mutated in cancers. Like other pleiotropic tumor suppressors, Fbw7's complex biology has impeded our understanding of how Fbw7 mutations promote tumorigenesis and hindered the development of targeted therapies. To address these needs, we employed a transfer learning approach to derive gene-expression signatures from The Cancer Gene Atlas datasets that predict Fbw7 mutational status across tumor types and identified the pathways enriched within these signatures. Genes involved in mitochondrial function were highly enriched in pan-cancer signatures that predict Fbw7 mutations. Studies in isogenic colorectal cancer cell lines that differed in Fbw7 mutational status confirmed that Fbw7 mutations increase mitochondrial gene expression. Surprisingly, Fbw7 mutations shifted cellular metabolism toward oxidative phosphorylation and caused context-specific metabolic vulnerabilities. Our approach revealed unexpected metabolic reprogramming and possible therapeutic targets in Fbw7-mutant cancers and provides a framework to study other complex, oncogenic mutations.

metabolism | ubiquitin | Fbw7 | genomics | informatics

Current technologies afford genome-scale characterization of the mutational and transcriptional landscape of thousands of human tumors, enabling a shift toward a taxonomy of cancer and targeted therapies based upon molecular criteria. The ability to reclassify tumors across organ sites based on shared mutations implies that driver mutations deregulate common oncogenic pathways across tissue types. However, many commonly mutated cancer genes (e.g., c-Myc, p53) regulate diverse processes, and their complex biology has confounded mechanistic studies of carcinogenesis and targeted therapy development. We thus explored the hypothesis that gene-expression signatures that predict a tumor's mutational status for a specific gene across organ sites may reveal insights into these types of oncogenic mutations. Toward this goal, we employed a machine-learning technique, kernelized Bayesian transfer learning (KBTL), to infer transcriptional signatures predictive of mutation status across multiple tumor types profiled in The Cancer Genome Atlas (TCGA) datasets (1).

Fbw7 is the substrate receptor of a Skp1–F-box–Cullin ubiquitin ligase that targets a network of substrates for proteasomal degradation after they become phosphorylated (2–5). Many Fbw7 substrates are oncoproteins, and Fbw7 is one of the most commonly mutated human tumor suppressors (3, 4, 6, 7). Heterozygous missense mutations that target one of three key Fbw7 arginine residues that interact with substrate phosphates (R465, R479, or R505; hereafter referred to as "Fbw7^{ARG}") are the most common Fbw7 mutations. Fbw7^{ARG} are thought to be dominant-negative alleles, but the mechanisms driving their selection are poorly understood (3, 8). Because many Fbw7 substrates are master transcription factors (TFs), Fbw7 mutations may broadly impact gene expression. Moreover, Fbw7-associated tumorigenesis likely involves the combinatorial activities of multiple stabilized oncoproteins rather than a single oncogenic driver. We thus chose Fbw7 as a test case of a complex and poorly understood cancer gene to study through the use of KBTL. We developed gene-expression signatures that predict Fbw7 mutational status and identified the biologic pathways enriched within Fbw7 predictive signatures, with the goal of developing insights into these mutations. Our approach revealed unexpected metabolic reprogramming and possible therapeutic targets in Fbw7-mutant cancer cells and provides a framework to study other complex oncogenic mutations.

Results

Inferring Cross-Tissue Transcriptional Signatures Associated with Cancer Gene Mutations. We adapted the KBTL methodology that we recently developed (1) to discriminate mutation-associated transcriptional processes shared across tumor types (Fig. 1 *A* and *B*). KBTL allows multiple related prediction tasks to be solved jointly by projecting feature matrices from each task onto a shared low-dimensional subspace inferred to yield high predictive accuracy across tasks. In the current application, we treat each tumor type as a separate task and infer gene-expression–based predictors of the mutation status of a given gene in each tumor type, using KBTL to identify gene-expression patterns (i.e., low-dimensional projections of the gene

Significance

Tumor suppression by the Fbw7 ubiquitin ligase remains poorly understood. Here, we used informatics and engineered cancer cells to show that Fbw7 mutations cause metabolic reprogramming by increasing oxidative phosphorylation and metabolic vulnerabilities that may represent therapeutic targets. Our approach may be applied to study other complex cancer genes.

Author contributions: R.J.D., M.G., D.H.M., P.J.P., D.R., J.E.G., D.M.H., A.A.M., and B.E.C. designed research; R.J.D., M.G., D.H.M., S.H., J.S., P.H., H.G., J.E.G., and B.E.C. performed research; J.E.G. contributed new reagents/analytic tools; R.J.D., M.G., D.H.M., S.H., J.S., H.G., D.R., A.A.M., and B.E.C. analyzed data; and R.J.D., M.G., D.H.M., J.S., D.M.H., A.A.M., and B.E.C. wrote the paper.

The authors declare no conflict of interest.

This article is a PNAS Direct Submission.

[1]R.J.D., M.G., and D.H.M. contributed equally to this work.

[2]D.M.H., A.A.M., and B.E.C. contributed equally to this work.

[3]To whom correspondence should be addressed. Email: bclurman@fredhutch.org.

This article contains supporting information online at www.pnas.org/lookup/suppl/doi:10.1073/pnas.1718338115/-/DCSupplemental.

Published online May 7, 2018.

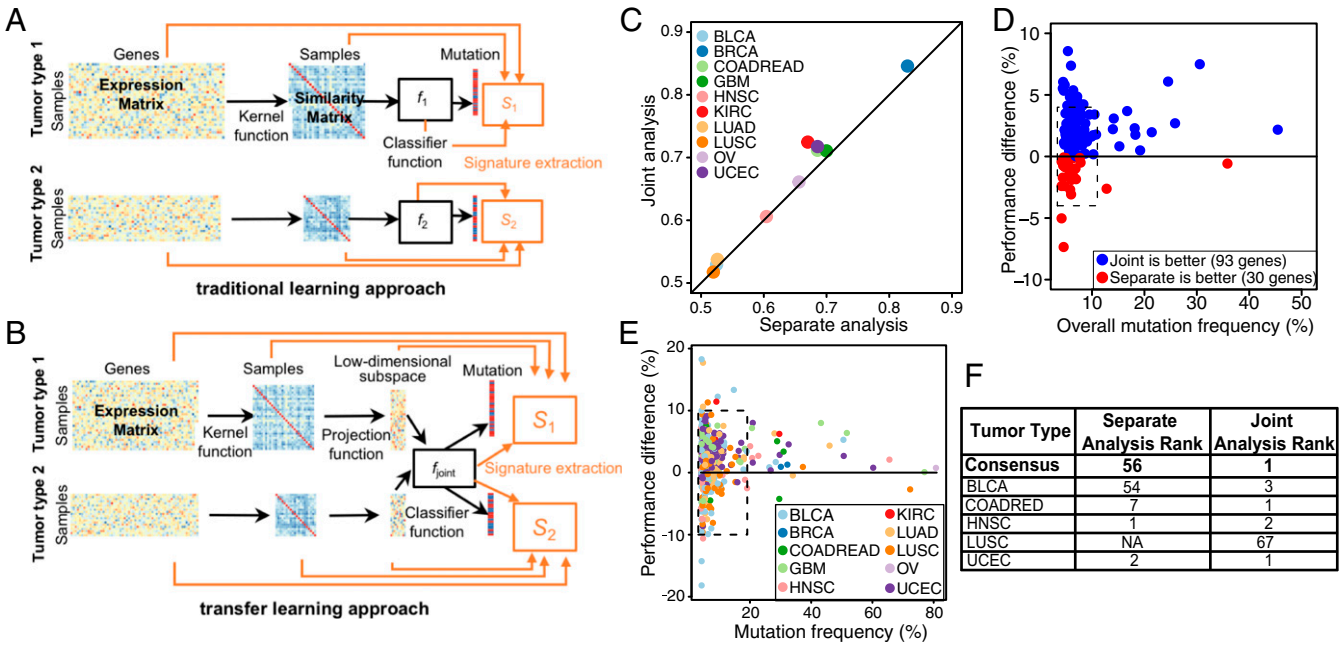

Tumor Type	Separate Analysis Rank	Joint Analysis Rank
Consensus	**56**	**1**
BLCA	54	3
COADRED	7	1
HNSC	1	2
LUSC	NA	67
UCEC	2	1

Fig. 1. KBTL improves predictive power for commonly mutated cancer genes and reveals enriched mitochondrial-associated gene expression in pan-cancer Fbw7 predictive signatures. (*A* and *B*) Depiction of single-task kernel-based learning (*A*) and KBTL (*B*) approaches used to develop gene-expression signatures that predict the mutational status of a specific gene from single tumor types, versus conjoint Pan-cancer analyses, respectively (see text and *SI Materials and Methods*). (*C*) Classification accuracy [area under the receiver operator characteristic curve (AUROC)] for separate analysis (RVM, *x* axis) vs. joint analysis (KBTL, *y* axis). Results are averaged across all genes for each tumor type. (*D*) Average mutation frequency of each gene (*x* axis) vs. percent improvement in classification accuracy (AUROC) for KBTL vs. RVM. Results are averaged across all tumor types for each gene weighted with cohort sizes. (*E*) Average mutation frequency of each gene (*x* axis) vs. percent improvement in classification accuracy (AUROC) for KBTL vs. RVM. Results are displayed for each gene type/tumor type pair. (*F*) Ranking of the mitochondrial module for each tumor type and consensus ranking across tumor types based on RVM (separate analysis) and KBTL (joint analysis). NA, not available.

expression matrices) that are associated with mutation status across all tumor types.

We analyzed 10 different tumor types and inferred predictive models of the mutational status of all genes with mutation rates >4% in at least 2 of the 10 tumor types (123 genes), as determined from the Cancer Gene Census (https://cancer.sanger.ac.uk/census/) (9). We assessed whether using KBTL to share information across tumor types yielded signatures with increased accuracy in predicting mutation status compared with analyzing each tumor type independently. KBTL has two potential advantages over traditional learning approaches: (*i*) increased statistical robustness, due to the larger sample size resulting from combining multiple datasets during learning, and (*ii*) the ability to extract signals that are common across datasets, which may reveal shared biological processes across organ sites. For each gene mutation/tumor type combination, we compared the pan-cancer KBTL-derived signatures (multitask learning; see *SI Materials and Methods*) with those obtained using the relevance vector machine (RVM), which is analogous to KBTL applied to each tumor type in isolation (single-task learning; see *SI Materials and Methods*) (10). KBTL improved prediction accuracy compared with RVMs for 9 of 10 (90%) tumor types averaged over all genes and for 93 of 123 (76%) genes averaged over tumor types (Fig. 1 *C* and *D* and Dataset S1). Overall, KBTL yielded improvements for 291 of 430 (68%) gene mutation/tumor type pairs. KBTL yielded improved performance for 27 of 30 (90%) of gene mutation/tumor type pairs with greater than 20% mutation frequency and for 66 of 81 (81%) gene mutation/tumor type pairs with greater than 10% mutation frequency (Fig. 1*E*). Most gene mutation/tumor type pairs for which KBTL did not yield improved performance demonstrated low mutational frequencies, suggesting insufficient positive samples for inference of classifiers. Conjoint modeling was especially useful in predicting the status of commonly mutated genes with known importance in carcinogenesis (e.g., TP53, KRAS, and PIK3CA) (Dataset S1).

Fbw7 Predictive Signatures Are Enriched for Genes Associated with Mitochondria. Five TCGA organ sites had sufficient *FBXW7*-mutant samples (>4%) for KBTL analyses: bladder urothelial carcinoma (BLCA), colon and rectum adenocarcinomas (COADREAD), head and neck squamous cell carcinoma (HNSC), lung squamous cell carcinoma (LUSC), and uterine corpus endometrial carcinoma (UCEC). We modeled all five tumor types individually or conjointly using KBTL to derive transcriptional signatures inferred to predict Fbw7 mutational status. To identify biological pathways enriched within these signatures, we performed gene set enrichment analysis (GSEA) of the 500 most predictive genes (of 20,530 total transcripts) using the DAVID 6.8 platform (https://david.ncifcrf.gov). Surprisingly, KBTL revealed that genes associated with mitochondrial function (hereafter termed "mitochondrial signature genes" or "MSGs") were the dominant biologic processes enriched within Fbw7 predictive gene signatures across tumor types (Fig. 1*F*). Dataset S2 shows the complete DAVID 6.8 analysis for COADREAD. In contrast, when analyzed by single-task learning, MSGs ranked as the 56th most enriched gene set associated with Fbw7 mutations averaged across tumor types.

Some tumor types, including glioblastomas, breast cancers, and ovarian cancers, exhibit Fbw7 mRNA repression rather than Fbw7 mutations (11–13). To determine if MSGs were similarly associated with Fbw7 loss via mRNA repression, we developed single-task transcriptional signatures predictive of the 10% of tumors with the lowest amount of Fbw7 expression in each organ site (Dataset S3). Remarkably, MSGs were the most highly enriched feature in each of these signatures, suggesting that Fbw7 loss caused by either mutations or reduced mRNA expression is widely associated with metabolic dysregulation in primary tumors.

Fbw7 Mutations Increase Mitochondrial Gene Expression in Colorectal Cancer Cell Lines. Due to the robust predictive power of the MSG module, we sought to validate a direct relationship between Fbw7 mutations and increased MSG expression. We focused on

colorectal cancer (CRC), which is the most prevalent Fbw7-associated cancer for which KBTL identified MSGs as the top-ranked enriched process (Fig. 1*F*). To establish a causal relationship between Fbw7 mutations and MSG expression, we generated isogenic CRC cell line panels that differed in Fbw7 status by mutating the endogenous *FBXW7* locus through adeno-associated virus (AAV) gene targeting (Fig. S1) (14). We engineered Hct116 cells, which are normally $Fbw7^{+/+}$, to contain either a heterozygous $Fbw7^{ARG}$ mutation ($Fbw7^{+/R505C}$) or a homozygous null mutation ($Fbw7^{-/-}$) (Fig. 2*A*) (14). Conversely, we engineered LoVo, a CRC cell line with a natural $Fbw7^{R505C/+}$ mutation, to correct the mutant allele and revert these cells to $Fbw7^{+/+}$ (two independent clones, A and B, were derived to reduce clonal selection artifacts) (Fig. 2*A*). Finally, we made $Fbw7^{+/R505C}$ and $Fbw7^{-/-}$ mutations in DLD1, another $Fbw7^{+/+}$ CRC cell line. Together, these cell panels provided complementary systems in which Fbw7 function was either impaired (Hct116 and DLD1) or restored (LoVo).

We previously characterized Fbw7 substrates in Fbw7-mutant Hct116 cells and extended these analyses to include these cell lines (14, 15). Cyclin E and Myc exhibit the largest Fbw7-dependent changes in CRC cell lines. Cyclin E abundance and its associated kinase activity (which specifically measures the pool of active cyclin E targeted by SCF^{Fbw7}) were greatly increased in $Fbw7^{-/-}$ cells (Fig. 2*B*). In contrast, $Fbw7^{R505/+}$ mutations caused small increases in cyclin E abundance and activity in Hct116 and DLD1 cells, and the LoVo revertants exhibited slightly reduced cyclin E activity compared with parental LoVo cells. Because c-Myc represses its own transcription, Fbw7 mutations that prolong Myc turnover may not increase c-Myc steady-state abundance, and c-Myc turnover is the most sensitive assay for its degradation by Fbw7 (14, 15). $Fbw7^{-/-}$ cells exhibited substantial c-Myc stabilization, whereas $Fbw7^{R505C/+}$ cells exhibited intermediate Myc stability (Fig. 2*C*). These findings are consistent with the modest Myc stabilization seen when Fbw7 dimerization is prevented, because $Fbw7^{ARG/+}$ mutations reduce the amount of dimeric WT-Fbw7 (15). Other substrates were not appreciably changed by $Fbw7^{ARG/+}$ mutations. We were unable to detect PGC-1α protein in any of these cell lines (Fig. S1*C*).

To determine the role of Fbw7 in regulating MSGs, we measured the expression of a panel of MSGs in the isogenic Hct116 and LoVo series. Compared with parental Hct116 cells, both the $Fbw7^{ARG/+}$ and $Fbw7^{-/-}$ Hct116 cell lines exhibited increased MSG expression (Fig. 2). Conversely, the restoration of normal Fbw7 function in LoVo cells reduced MSG expression in both gene-targeted clones (Fig. 2*E*). These studies validated the KBTL prediction that Fbw7 mutations directly increase MSG expression, which is conserved from primary tumors to cell lines.

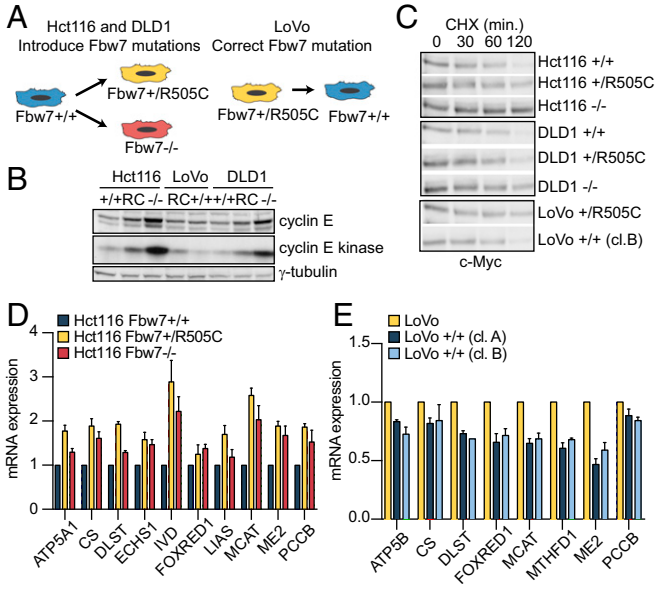

Fig. 2. Fbw7 mutations increase gene expression of mitochondrial signature genes. (*A*) Schema depicting the generation of isogenic Hct116, DLD1, and LoVo cell lines with wild-type and mutated Fbw7 (see Fig. S1 for the engineering strategy). (*B*). Cyclin E abundance and cyclin E-associated kinase assay in isogenic cell lines. (*C*) Myc decay in cell line panels. Cycloheximide (CHX,100 μg/mL) was added as indicated. (*D*) Quantitative RT-PCR analysis of a subset of mitochondrial signature gene mRNAs in gene-targeted Hct116 cells: $Fbw7^{+/+}$, $Fbw7^{+/R505C}$, and $Fbw7^{-/-}$. Data represent the means ± SEM of at least two biological replicates. (*E*) MSG mRNA analyses as in *D* in gene-targeted isogenic LoVo cell lines. Data represent the means ± SEM of at least two biological replicates. cl, clone; min, minutes.

Fbw7 Regulates Mitochondrial Function in CRC Cells. Having demonstrated deregulated MSG expression in Fbw7-mutant cells, we next determined if Fbw7 mutations alter cellular metabolism. We measured oxygen-consumption rates (OCR) and extracellular acidification rates (ECARs), which reflect oxidative and glycolytic metabolism, respectively. In both the Hct116 and LoVo panels, basal and maximal OCR, as revealed by the addition of the uncoupling agent carbonyl cyanide-4-(trifluoromethoxy) phenylhydrazone (FCCP), were significantly higher in $Fbw7^{ARG/+}$ and $Fbw7^{-/-}$ cells than in $Fbw7^{+/+}$ cells (Fig. 3 *A* and *B*). We also observed Fbw7-dependent OCR changes in DLD1 cells (Fig. 3*C*). Basal ECARs were lower in LoVo cells than in $Fbw7^{+/+}$-reverted LoVo cells but were higher in $Fbw7^{ARG/+}$ and $Fbw7^{-/-}$ Hct116 cell lines than in parental $Fbw7^{+/+}$ Hct116 cells (Fig. S2 *A* and *B*). To investigate these differences, we compared OCR responses to the addition of glutamine, an alternative respiratory substrate in cancer cells via glutaminolysis (Fig. 3 *G* and *H*). Glutamine addition stimulated the OCR to a greater extent in $Fbw7^{ARG}$ and $Fbw7^{-/-}$ Hct116 cells than in parental cells but failed to stimulate the OCR in $Fbw7^{+/ARG}$ LoVo cells compared with reverted $Fbw7^{+/+}$ cells. Together, these results suggest that increased respiration in Fbw7-deficient cancer cells is associated with different fuel choices in Hct116 cells (glutamine) and LoVo cells (glucose).

Increased OCR/ECAR ratios indicate a shift from glycolytic to oxidative metabolism. Accordingly, Fbw7-mutant LoVo, Hct116, and DLD1 cell lines all had higher OCR/ECAR ratios than did wild-type controls (Fig. 3 *D*–*F*). To reduce the chance of clonal artifacts during AAV targeting, we also impaired Fbw7 function by using shRNA to reduce Fbw7 expression in DLD1 cells and HT-29 cells (another $Fbw7^{+/+}$ CRC cell line) and by CRISPR/Cas9 to genetically ablate Fbw7 in Hct116 cells (*SI Materials and Methods* and Fig. S2 *C*–*F*). Finally, we extended these studies beyond CRC and used shRNA to knock down Fbw7 expression in G14 cells, a glioblastoma (GBM) stem cell line (Fig. S2 *G*–*I*) (16). In each case, reduced Fbw7 function increased the OCR/ECAR ratio. Thus, Fbw7 mutations are not associated with the Warburg effect (aerobic glycolysis) common to many cancers but instead cause a shift toward mitochondrial respiration.

Metabolic Consequences of Fbw7 Mutations in CRC Cells. Global metabolite profiles revealed Fbw7-dependent metabolic changes in greater detail. Principal component analyses separated Hct116 and LoVo cells according to Fbw7 status, indicating that metabolite profiles track with Fbw7 function (Fig. S3 *A* and *C*). Univariate analyses of the Hct116 metabolome revealed increased abundance of serine, glycine, creatine, and the serine metabolite glycerate and decreased abundance of lactate and glutamine in both $Fbw7^{ARG/+}$ and $Fbw7^{-/-}$ cells (Fig. 4*A* and Dataset S4). These changes are consistent with increased glutaminolysis and possibly serine biosynthesis, a glycolysis-diverting pathway. In contrast, Fbw7-mutant LoVo cells displayed a strong signature of increased glycolytic intermediates: metabolite set enrichment analysis identified glycolysis (up), purine metabolism (up), and glycine, serine, and threonine metabolism (down) as metabolic pathways with significant differences [false-discovery rate (FDR) = 0.037, 0.039, and 0.0498, respectively] (Fig. 4*B*, Fig. S3*D*, and Dataset S4). The tricarboxylic acid (TCA) cycle intermediate aconitate was highly elevated in parental Fbw7-mutant LoVo cells compared with wild-type

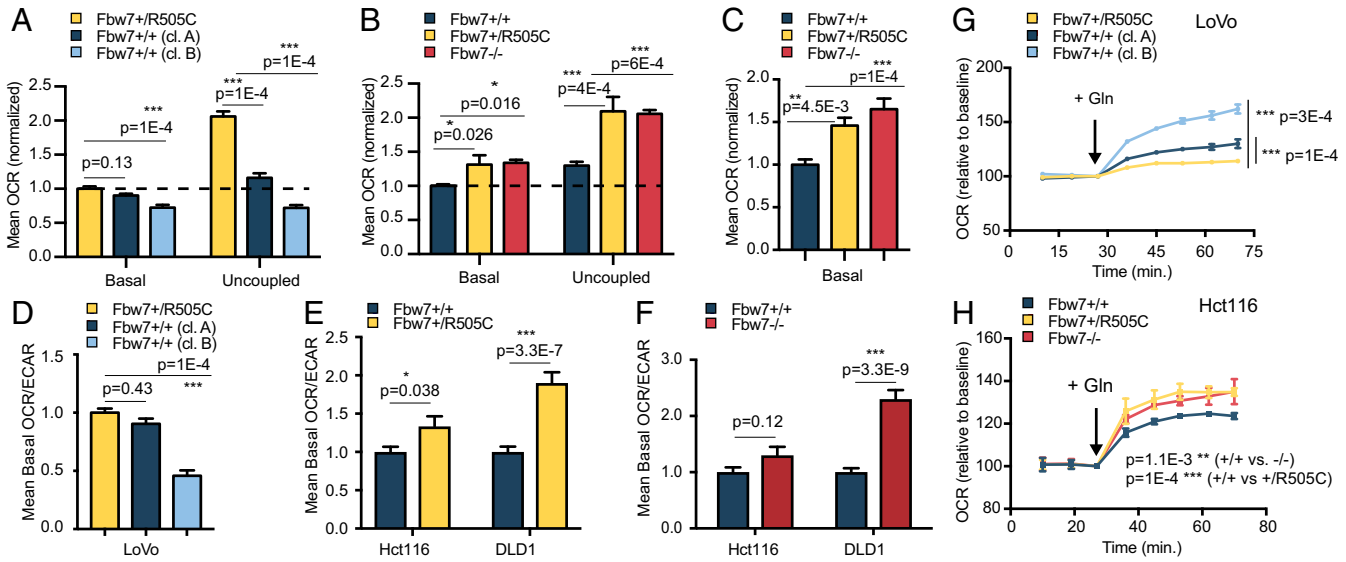

Fig. 3. Fbw7-mutant CRC cells exhibit increased oxidative metabolism and context-dependent changes in central carbon metabolism. (*A*) Basal and uncoupled OCRs of isogenic LoVo cell lines. Basal OCR: $P < 0.0001$, one-way ANOVA; uncoupled OCR: $P < 0.0001$, one-way ANOVA 1. Multiplicity-adjusted *P* values from post hoc analysis using Dunnett's multiple comparisons test are indicated. (*B*) As in *A* for isogenic Hct116 cell lines. Basal OCR: $P = 0.0143$, one-way ANOVA; uncoupled OCR: $P = 0.0002$, one-way ANOVA. (*C*) Analysis similar to that in *A* for isogenic DLD1 cell lines. Basal OCR: $P = 0.0002$, one-way ANOVA. (*D*) OCR/ECAR ratios under basal conditions in isogenic LoVo cell lines. $P < 0.0001$, one-way ANOVA. (*E*) Analysis similar to that shown in *D* comparing isogenic Hct116 and DLD1 cell lines; *P* values from unpaired *t* tests are indicated. (*F*) Analysis similar to that in *D* comparing isogenic Hct116 and DLD1 cell lines. (*G* and *H*) Effect of acute glutamine addition (2 mM) on OCRs. Changes are presented as increases above baseline OCRs in glutamine-free medium. $P < 0.0001$, one-way ANOVA for all time points following glutamine addition in LoVo (*G*) and Hct116 (*H*) cell lines. Data represent the means ± SEM of at least two independent biological replicates, each with four to five technical replicates. Multiplicity-adjusted *P* values from post hoc analysis using Dunnett's multiple comparisons test are indicated. Asterisks in all panels denote significance as follows: $*P < 0.05$, $**P < 0.01$, $***P < 0.001$. cl, clone; min, minutes.

Fbw7 revertants. As LoVo Fbw7$^{R505C/+}$ cells have low ECARs and high OCRs, this supports the hypothesis that the Fbw7 mutation increases glucose delivery to mitochondrial oxidative metabolism.

U-^{13}C-glucose labeling was used to study Fbw7-dependent changes in glucose flux in Fbw7$^{-/-}$ and Fbw7$^{+/+}$ cells. Hct116 Fbw7-null cells showed an increased enrichment ratio for serine/lactate compared with Fbw7$^{+/+}$ cells, consistent with glycolytic diversion to serine biosynthesis (Fig. 4*C*). There was uniformly reduced labeling of TCA cycle metabolites, indicating that a mitochondrial fuel other than glucose sustained the higher OCR in Fbw7$^{-/-}$ Hct116 cells. In contrast, LoVo cells revealed a striking increase in glucose-derived carbon incorporation into TCA cycle metabolites in Fbw7-mutant compared with Fbw7-revertant cells, consistent with increased glucose oxidation (Fig. 4*E*). Total metabolite levels from the glucose-tracing experiments demonstrated higher citrate levels in parental LoVo cells and confirmed elevated serine levels in Fbw7$^{-/-}$ Hct116 cells (Fig. 4 *D* and *F*). The increased mitochondrial metabolism associated with Fbw7 loss can thus be sustained by oxidation of different carbon substrates, yielding distinct metabolic signatures in different cell types (Fig. 5).

Metabolic reprogramming in cancer cells may create therapeutic vulnerabilities. We therefore studied whether Fbw7 mutations sensitized CRC cell lines to metabolic inhibitors of the pathways implicated above. Serine is the metabolite that exhibits the greatest increase in Fbw7-mutant Hct116 cells but not in LoVo cells. Accordingly, Fbw7$^{-/-}$ Hct116 cells (but not LoVo cells) were highly sensitized to two inhibitors (NCT-503 and CBR-5886) of phosphoglycerate dehydrogenase (PHGDH), a critical enzyme in serine biosynthesis (Fig. 4*G* and Fig. S4*C*). The glycolytic diversion to serine in Hct116 cells lacking Fbw7 is thus required for cellular survival. Citrate is a donor of acetyl-CoA units for de novo fatty acid synthesis after export from mitochondria and is an allosteric activator of acetyl-CoA carboxylase. The Fbw7-dependent 10-fold increase in the citrate/α-ketoglutarate ratio in LoVo cells thus suggested a possible diversion of mitochondrial citrate for lipid biosynthesis. Indeed, Fbw7 regulates cholesterol and lipid metabolism via degradation of SREBP1 and C/EBPα (17, 18), and parental LoVo cells exhibited increased size and number of cytoplasmic lipid droplets compared with revertants (Fig. S4 *A* and *B*). Accordingly, inhibition of fatty acid synthesis with 5-(tetradecyloxy)-2-furoic acid (TOFA), an acetyl-CoA carboxylase-1 (ACC1) inhibitor, was more cytotoxic to LoVo Fbw7$^{+/R505C}$ cells than to either Fbw7-deficient Hct116 cells or corresponding Fbw7$^{+/+}$ cell lines (Fig. 4*H* and Fig. S4*F*). DLD1 cells also displayed Fbw7-dependent TOFA sensitivity, albeit to a lesser extent than seen in LoVo cells (Fig. S4 *C* and *D*). Fbw7 mutations may thus lead to context-specific metabolic vulnerabilities in cancer cells.

Discussion

We describe an approach to infer the physiologic consequences of oncogenic mutations in which we (*i*) derived gene-expression signatures from TCGA datasets that predict a gene's mutational status across different tumor types and (*ii*) identified the shared biologic pathways enriched within predictive signatures. The primary goal of using transfer learning to conjointly study multiple organ sites was to reveal the core consequences of mutations. Here, we validate this approach by demonstrating a previously unknown role of Fbw7 in the control of cellular metabolism. Given the increased predictive power of conjoint modeling for most common oncogenic mutations, this approach may be useful to study other pleiotropic cancer genes.

Several Fbw7 substrates regulate metabolism (e.g., PGC-1α, Myc, Notch, and SREBP), and it was not unexpected to find metabolic consequences of Fbw7 mutations. However, given Fbw7's prominent roles in processes such as proliferation and differentiation, it was surprising to discover that metabolism was the most highly conserved feature in Fbw7 predictive signatures. Perhaps most striking is the similar metabolic dysregulation caused by Fbw7$^{ARG/+}$ and Fbw7$^{-/-}$ mutations. Fbw7$^{ARG/+}$ mutations do not stabilize substrates to the same extent as Fbw7-null mutations (Fig. 2*E* and Fig. S1*C*), and with the possible exception of Myc in T-lineage acute lymphoblastic leukemia (19), the mechanisms driving Fbw7$^{ARG/+}$ selection remain unknown (3, 8). The similar bioenergetic consequences of Fbw7$^{ARG/+}$ and Fbw7$^{-/-}$ mutations thus suggest that metabolic reprogramming may, in part, underlie the Fbw7 mutational spectrum in cancers. This

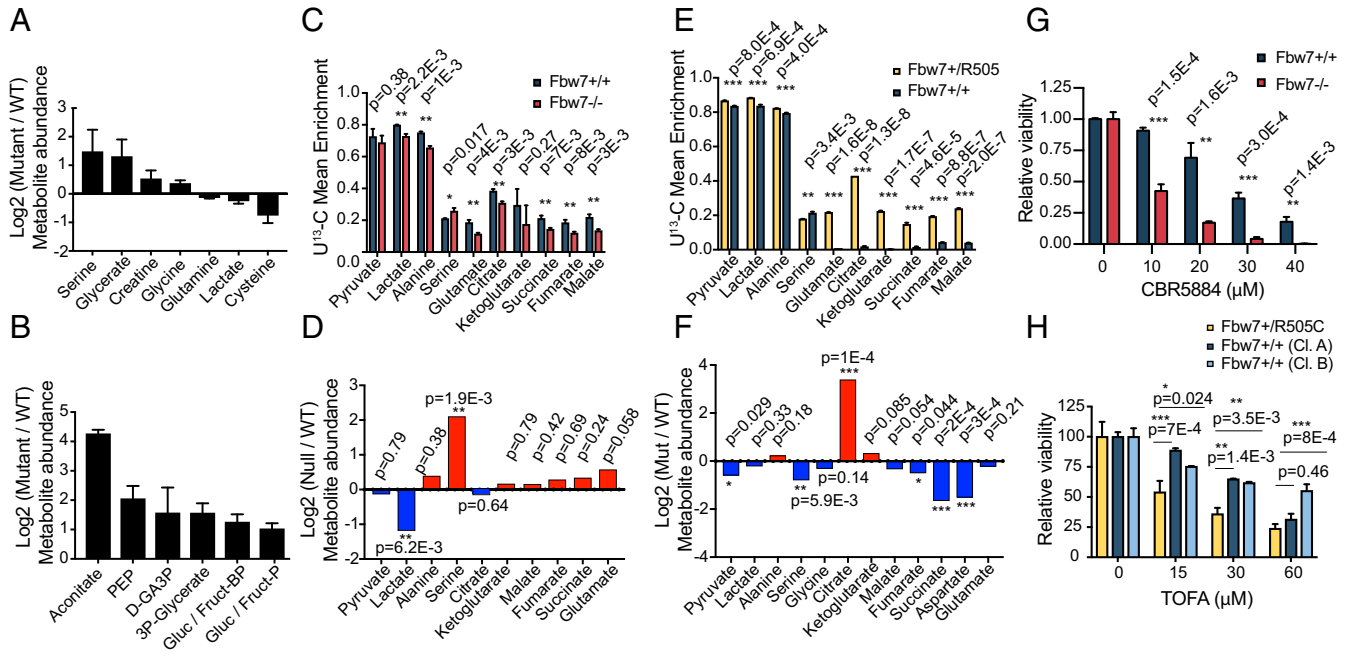

Fig. 4. Metabolite profiling and glucose flux analysis of isogenic cell lines reveal cell-type–specific metabolic alterations and vulnerabilities. (*A*) Log_2 fold change of metabolite abundances for a subset of metabolites whose abundance was significantly changed between Hct116 mutant and wild-type cell lines. (*B*) As in *A* but in LoVo cell lines. (*C*) Mean ^{13}C enrichment of Hct116 glycolysis intermediates, amino acids, and TCA cycle metabolites after U-^{13}C-glucose labeling. Data represent the means ± SEM of at least three biological replicates. *P* values from unpaired two-tailed *t* tests are indicated. (*D*) Steady-state log_2 ($Fbw7^{-/-}$/$Fbw7^{+/+}$) metabolite abundances for metabolites presented in *C*. (*E*) As in *C*, but for isogenic LoVo $Fbw7^{+/R505C}$ and $Fbw7^{+/+}$ (clone B) cell lines. (*F*) As in *D*, but for isogenic LoVo cell lines. (*G*) Cell viability following 6-d treatment of Hct116 $Fbw7^{+/+}$ and $Fbw7^{-/-}$ cells with the PHGDH inhibitor CBR5884. *P* values from unpaired two-tailed *t* tests are indicated. (*H*) LoVo cell viability following 48-h treatment with TOFA, an acetyl-CoA carboxylase inhibitor. (15 μM: $P = 0.0012$; 30 μM: $P = 0.0013$; 60 μM: $P = 0.0011$; all one-way ANOVA.) *P* values for Dunnett's multiple comparisons test are indicated. Viability data represent the means ± SEM of at least two biological replicates. Asterisks in all panels denote significance as follows: *$P < 0.05$, **$P < 0.01$, ***$P < 0.001$. cl, clone; min, minutes.

idea is further supported by the finding that MSGs are the most enriched feature of predictive signatures associated with low Fbw7 mRNA expression in solid tumors (Dataset S3). TF-binding site analyses did not implicate any single Fbw7 substrate as likely to be responsible for MSG deregulation in Fbw7-mutant cancers, and the metabolic phenotypes likely reflect the combined activities of multiple Fbw7 substrates. However, the specific contributions of individual substrates require further study.

Increased OCR is a common finding in Fbw7-deficient cells. However, rather than increasing the mitochondrial metabolism of a specific fuel, Fbw7 loss affords flexibility in fuel selection. Thus, while $Fbw7^{R505C/+}$ LoVo cells exhibit increased glucose oxidation, Hct116 cells with either $Fbw7^{R505C/+}$ or $Fbw7^{-/-}$ genotypes exhibit increased glutamine-stimulated respiration. These cell-type–specific effects argue against Fbw7 deficiency having direct effects on oxidation pathways for specific nutrients but instead that it increases mitochondrial activity (Fig. 5).

Metabolic deregulation caused by oncogenes is influenced by contexts such as cell lineage and other mutations. Both Hct116 and LoVo cells contain Kras mutations and activated β-catenin. However, Hct116 cells have a PIK3CA mutation and MYC amplification that increase glutaminolysis via glutamate pyruvate transaminase 2 expression and glutaminase expression, respectively, leading to glutamine dependence with enhanced alanine and oxoglutarate production and TCA-cycle anaplerosis (20). Furthermore, glutaminolysis provides a key intermediate for the serine biosynthetic pathway through the production of glutamate (21). The addition of an Fbw7 mutation to this genetic background augments glutamine oxidation and serine synthesis and creates a new vulnerability as cells become sensitive to PHGDH inhibition. The serine synthesis pathway is also essential in other oncogenic contexts, such as subsets of breast cancers and melanomas (22–24).

LoVo cell bioenergetics and central carbon metabolism have not been previously reported. Our data demonstrate an oxidative phenotype with increased glucose metabolism and citrate synthesis in $Fbw7^{ARG/+}$ LoVo parental cells. Correction of the Fbw7 mutation leads to dramatically reduced glucose oxidation and increased glutamine dependency. Metabolomics, ^{13}C-glucose tracer analysis, and lipid staining all point toward Fbw7-mediated channeling of glucose into lipid synthesis in LoVo cells, which may lead to their increased sensitivity to acetyl-CoA carboxylase inhibition. The metabolic dysregulation caused by Fbw7 mutations in different cellular contexts may thus allow new, targeted therapies.

The selective advantage of increased oxidative metabolism in Fbw7-deficient cells may depend on unique mitochondrial

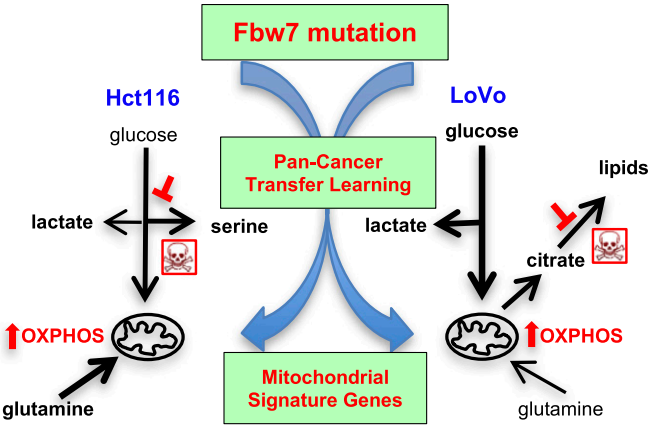

Fig. 5. Mitochondrial fuel utilization in Fbw7-deficient CRC cell lines. Thick arrows indicate increased fluxes caused by Fbw7 loss as implicated by bioenergetic, metabolomics, and tracer studies. Red inhibition symbols indicate metabolic vulnerabilities.

functions in anabolic metabolism. For example, citrate generated from glucose (via pyruvate dehydrogenase/pyruvate carboxylase) and glutamine (via reductive carboxylation) can be converted to cytosolic acetyl-CoA for fatty acid biosynthesis by ATP citrate lyase following mitochondrial export. The electron transport chain is also essential for the synthesis of aspartate, a precursor for pyrimidine nucleotide biosynthesis (25). Increased oxidative, rather than Warburg, metabolism has been reported in melanomas with MITF-induced PGC-1α expression and in B-cell lymphomas with dependencies on fatty acid oxidation (26, 27). Increased mitochondrial biogenesis and oxidative phosphorylation in cancer cells may also promote metastasis and is an important feature of circulating mammary epithelial cancer cells (28). Increased oxidative metabolism in Fbw7-deficient cells might thus impact cellular adaptation to the microenvironment, invasion, and differentiation.

Materials and Methods

Computational Methods. Ten TCGA datasets were analyzed: BLCA, BRCA, COADREAD, GBM, HNSC, kidney renal clear cell carcinoma, lung adenocarcinoma, LUSC, ovarian serous cystadenocarcinoma (OVCA), and UCEC (https://www.synapse.org/#!Synapse:syn300013). One hundred twenty-three cancer genes with mutation rates >4% in at least two tumor types were identified (https://cancer.sanger.ac.uk/census/) (9). For each gene mutation/tumor type pair, we inferred predictive models of mutation status based on gene expression by (*i*) modeling each cancer individually with the RVM and (*ii*) modeling all cancers conjointly with KBTL. GSEA analyses were performed using DAVID Bioinformatics 6.8 (https://david.ncifcrf.gov). See *SI Materials and Methods* and ref. 1 for KBTL/GSEA methodology.

Cell Culture, Antibodies, Western Blotting, Immunoprecipitation, and Kinase Assays. All cells were maintained in DMEM high-glucose medium (+10% FBS and penicillin/streptomycin) except for DLD1 cells (which were maintained in RPMI medium) and G14 cells (which were maintained as described in ref. 29). Antibodies are described in *SI Materials and Methods*. Immunoblotting and kinase assays were performed as previously described (30).

Cell Growth/Survival Assays. Cells were seeded in 96-well plates at 3,000 cells per well. The effects of the phosphoglycerate dehydrogenase inhibitors NCT-503 and CBR5884 (Sigma) and the acetyl-CoA carboxylase inhibitor TOFA (Sigma) on cell growth were determined via CellTiter-Glo (Promega) at 3–6 d after treatment.

Quantitative RT-PCR and Gene-Expression Analyses. Total RNA was extracted with TRIzol (Life Technologies) and purified using RNA Miniprep Kits (Zymo Research). Quantitative RT-PCR reactions were performed as described in *SI Materials and Methods*.

Seahorse Extracellular Flux Assays. Bioenergetic assays to measure OCRs and ECARs were performed using a Seahorse XF24 Bioanalyzer (Agilent). See *SI Materials and Methods* for experimental details.

Gene Targeting. Hct116 Fbw7$^{-/-}$ gene targeting has been previously described, and DLD1 Fbw7-null cells were made using the same methods (14). All clones were verified by Southern blotting, PCR, and genomic sequencing. Hct116 Fbw7$^{+/R505C}$ cells and LoVo Fbw7$^{+/+}$ cells were generated using analogous methods (*SI Materials and Methods* and Fig. S1). For CRISPR-Cas9–mediated knockout of FBXW7, single-guide RNAS (sgRNAs) were cloned into pLentiCRISPR_v2 (sgFBXW7: 5′-AAGAGCGGACCTCAGAACCA-3′; sgCtl: 5′-GTAGCGAACGTGTCCGGCGT-3′). Cells were transduced with lentiviruses and were selected with puromycin, and clones were isolated by limiting dilution. Fbw7 protein loss was examined by immunoprecipitation/Western blotting (Fig. S3).

Metabolite Profiling and Flux Experiments. Metabolites were extracted and analyzed in the Northwest Metabolomics Research Center as described in *SI Materials and Methods* and refs. 31 and 32. See *SI Materials and Methods* for U-^{13}C-glucose flux experiments. Metabolite profiling was analyzed with MetaboAnalyst 3.0 (www.metaboanalyst.ca) after normalization by protein and total intensity current.

Statistical Analysis. Statistical significance was determined using unpaired two-tailed Student's *t* test for two-group comparisons and one-way ANOVA followed by Dunnett's multiple comparison test to compare data from multiple groups.

ACKNOWLEDGMENTS. We thank Jeff Delrow for expert gene-expression guidance. The work was supported by National Cancer Institute Cancer Center Support Grants P30CA015704-40, U01CA217862, and U54CA209988 (to A.A.M.), R01CA190957 (to P.J.P.), and R01 CA193808 (to B.E.C.) and by the Turkish Academy of Sciences and the Science Academy of Turkey (M.G.).

1. Gonen M, Margolin A (2014) Kernelized Bayesian transfer learning. *Proceedings of the 28th AAAI Conference on Artificial Intelligence*. Available at https://www.aaai.org/ocs/index.php/AAAI/AAAI14/paper/view/8132/8817. Accessed April 13, 2018.
2. Ang XL, Wade Harper J (2005) SCF-mediated protein degradation and cell cycle control. *Oncogene* 24:2860–2870.
3. Davis RJ, Welcker M, Clurman BE (2014) Tumor suppression by the Fbw7 ubiquitin ligase: Mechanisms and opportunities. *Cancer Cell* 26:455–464.
4. Kourtis N, Strikoudis A, Aifantis I (2015) Emerging roles for the FBXW7 ubiquitin ligase in leukemia and beyond. *Curr Opin Cell Biol* 37:28–34.
5. Skaar JR, Pagan JK, Pagano M (2013) Mechanisms and function of substrate recruitment by F-box proteins. *Nat Rev Mol Cell Biol* 14:369–381.
6. Akhoondi S, et al. (2007) FBXW7/hCDC4 is a general tumor suppressor in human cancer. *Cancer Res* 67:9006–9012, and erratum (2008) 68:1245.
7. Kandoth C, et al. (2013) Mutational landscape and significance across 12 major cancer types. *Nature* 502:333–339.
8. Davis H, Tomlinson I (2012) CDC4/FBXW7 and the 'just enough' model of tumourigenesis. *J Pathol* 227:131–135.
9. Futreal PA, et al. (2004) A census of human cancer genes. *Nat Rev Cancer* 4:177–183.
10. Tipping ME (2001) Sparse bayesian learning and the relevance vector machine. *J Mach Learn Res* 1:211–244.
11. Hagedorn M, et al. (2007) FBXW7/hCDC4 controls glioma cell proliferation in vitro and is a prognostic marker for survival in glioblastoma patients. *Cell Div* 2:9.
12. Wei G, Wang Y, Zhang P, Lu J, Mao JH (2012) Evaluating the prognostic significance of FBXW7 expression level in human breast cancer by a meta-analysis of transcriptional profiles. *J Cancer Sci Ther* 4:299–305.
13. Kitade S, et al. (2016) FBXW7 is involved in the acquisition of the malignant phenotype in epithelial ovarian tumors. *Cancer Sci* 107:1399–1405.
14. Grim JE, et al. (2008) Isoform- and cell cycle-dependent substrate degradation by the Fbw7 ubiquitin ligase. *J Cell Biol* 181:913–920.
15. Welcker M, et al. (2013) Fbw7 dimerization determines the specificity and robustness of substrate degradation. *Genes Dev* 27:2531–2536.
16. Toledo CM, et al. (2015) Genome-wide CRISPR-Cas9 screens reveal loss of redundancy between PKMYT1 and WEE1 in glioblastoma stem-like cells. *Cell Rep* 13:2425–2439.
17. Bengoechea-Alonso MT, Punga T, Ericsson J (2005) Hyperphosphorylation regulates the activity of SREBP1 during mitosis. *Proc Natl Acad Sci USA* 102:11681–11686.
18. Bengoechea-Alonso MT, Ericsson J (2010) The ubiquitin ligase Fbxw7 controls adipocyte differentiation by targeting C/EBPalpha for degradation. *Proc Natl Acad Sci USA* 107:11817–11822.
19. King B, et al. (2013) The ubiquitin ligase FBXW7 modulates leukemia-initiating cell activity by regulating MYC stability. *Cell* 153:1552–1566.
20. Hao Y, et al. (2016) Oncogenic PIK3CA mutations reprogram glutamine metabolism in colorectal cancer. *Nat Commun* 7:11971.
21. Amelio I, Cutruzzolá F, Antonov A, Agostini M, Melino G (2014) Serine and glycine metabolism in cancer. *Trends Biochem Sci* 39:191–198.
22. Locasale JW, Cantley LC (2011) Genetic selection for enhanced serine metabolism in cancer development. *Cell Cycle* 10:3812–3813.
23. Possemato R, et al. (2011) Functional genomics reveal that the serine synthesis pathway is essential in breast cancer. *Nature* 476:346–350.
24. Mattaini KR, Sullivan MR, Vander Heiden MG (2016) The importance of serine metabolism in cancer. *J Cell Biol* 214:249–257.
25. Birsoy K, et al. (2015) An essential role of the mitochondrial electron transport chain in cell proliferation is to enable aspartate synthesis. *Cell* 162:540–551.
26. Caro P, et al. (2012) Metabolic signatures uncover distinct targets in molecular subsets of diffuse large B cell lymphoma. *Cancer Cell* 22:547–560.
27. Vazquez F, et al. (2013) PGC1α expression defines a subset of human melanoma tumors with increased mitochondrial capacity and resistance to oxidative stress. *Cancer Cell* 23:287–301.
28. LeBleu VS, et al. (2014) PGC-1alpha mediates mitochondrial biogenesis and oxidative phosphorylation in cancer cells to promote metastasis. *Nat Cell Biol* 16:992–1003, 1–15.
29. Toledo LI, et al. (2011) A cell-based screen identifies ATR inhibitors with synthetic lethal properties for cancer-associated mutations. *Nat Struct Mol Biol* 18:721–727.
30. Welcker M, et al. (2003) Multisite phosphorylation by Cdk2 and GSK3 controls cyclin E degradation. *Mol Cell* 12:381–392.
31. Zhu J, et al. (2014) Colorectal cancer detection using targeted serum metabolic profiling. *J Proteome Res* 13:4120–4130.
32. Carroll PA, et al. (2015) Deregulated Myc requires MondoA/Mlx for metabolic reprogramming and tumorigenesis. *Cancer Cell* 27:271–285.